2

Growth and Characterization of Ytterbium Doped Silicate Crystals for Ultra-Fast Laser Applications

Lihe Zheng, Liangbi Su and Jun Xu
Shanghai Institute of Ceramics, Chinese Academy of Sciences, P. R. China

1. Introduction

Diode-pumped solid-state lasers (DPSSL) have predominated over waveguide lasers and fiber lasers when considering the efficiency and operability since the first realization of laser-diode pumped Yb-doped laser at room temperature (Lacovara et al., 1991). As a rule of thumb, DPSSL are preferable for devices operating with high peak power, whereas low-threshold and high-gain operation is much easier to be achieved with waveguide lasers and amplifiers. Besides the application in the fields of double-frequency, remote sensing and biomedical, ultra-fast DPSSL with diversified wavelength and stable system is widely exploited in the fields of mechanics, micro-electrics and ultra-fast photo-communication. DPSSL are composed of laser resonator which is mostly formed with discrete laser mirrors placed around gain medium with an air space in between. Bulk crystals or glasses doped either with rare earth ions or transition-metal ions are adopted as gain medium. With the development of DPSSL industries, the demand for laser crystals with the advantageous physicochemical properties such as efficient energy absorption, high optical uniformity and favorable thermal behavior has dramatically increased over the past few decades (Keller, 2003). With the rapid development of InGaAs laser diodes emitting from 900nm to 980nm, Yb^{3+} doped laser crystals are expected to alternate the traditional Nd^{3+} doped for generating efficient broad tunable and ultra-fast DPSSL in near-IR spectral range (Krupke, 2000).

Yb^{3+} ion with simple quasi-three energy level scheme of $^2F_{7/2}$ and $^2F_{5/2}$ is provided with high quantum efficiency, long lifetime of metastable $^2F_{5/2}$ level and large crystal-field splitting which is beneficial for reducing thermal load and enhancing Yb^{3+} doping level bringing about the realization of compact device without luminescence quenching caused by cross relaxation and excited-state absorption (Giesen & Speiser, 2007; Pelenc et al., 1995). However, the strong re-absorption at emission wavelengths leads to high pump threshold since the thermally populated terminal level of Yb^{3+} lasers at the ground state manifold is contemporary the laser terminal level. To reduce the re-absorption losses at laser emission wavelengths, strong splitting of ground sublevels of $^2F_{7/2}$ in Yb^{3+} ion is required to form a quasi-four-level system as that of Nd^{3+}. Thus, laser crystal hosts with low symmetry structure and strong crystal field splitting are the central issues in exploiting new Yb doped gain media (Du et al., 2006). Crystal hosts such as aluminum, tungsten, oxides, fluorides and

vanadates were explored for diode-pumped ultra-fast lasers (Uemura & Torizuka, 2005; Liu et al., 2001; Griebner et al., 2004; Su et al., 2005; Kisel et al., 2005).
The chapter is devoted to the systematical investigation on Yb doped oxyorthosilicate crystals such as gadollinium silicate (Gd_2SiO_5, GSO), yttrium silicate (Y_2SiO_5, YSO), Lutetium silicate (Lu_2SiO_5, LSO) and scandium silicate (Sc_2SiO_5, SSO) obtained by the Czochralski Crystal Growth System with Automatic Diameter Control, which encompassing distinctive low symmetry monoclinic structure, excellent physicochemical properties and favorable spectroscopic features for DPSSL. Besides, the chapter summarizes the structure properties of the obtained silicate crystals. Afterwards the chapter discusses the optical properties of silicate crystals available for ultra-fast lasers, together with the calculation of spectroscopic parameters such as pump saturation intensities I_{sat}, minimum pump intensities I_{min} and gain spectra of laser medium. Finally, the laser performance of the studied silicates is briefly outlined.

2. Experimental details of silicate crystals

The basic properties of rare earth oxyorthosilicate crystals were presented in Table 1*. Silicate Crystals were obtained by Czochralski method. Structure and spectra method were outlined as well as the laser experiments in the following elaboration.

2.1 Basic properties of rare earth oxyorthosilicate crystals

The monoclinic orthosilicate crystals RE_2SiO_5 could be stably formed according to the binary phase diagram of RE_2O_3-SiO_2, where RE stands for Lu^{3+}, Gd^{3+}, Y^{3+} and Sc^{3+}. RE^{3+} ions occupy two different low symmetry crystallographic sites which Yb^{3+} ion could substitute with selectively. The Rare Earth silicates with larger Rare Earth ion radius from La^{3+} to Tb^{3+} manifest the space group of $P2_1/c$ with typical compounds of La_2SiO_5 and GSO, while those with smaller Rare Earth ion radius from Dy^{3+} to Lu^{3+} as well as Y^{3+} and Sc^{3+} hold the space group of C2/c with typical compound of YSO and LSO.
Researchers show solitude for the crystal growth, structure, opto-electrical properties on Rare Earth doped RE_2SiO_5 crystals (Eijk, 2001; Kuleshov et al., 1997; Melcher & Schweitzer, 1992; Ivanov et al., 2001). Table 1 reveals the comparison of the basic physicochemical properties of monoclinic silicate crystals (Gaume, 2002; Smolin & Tkachev, 1969; Camargo et al., 2002). As seen from Table 1, LSO, YSO and SSO crystals are with Monoclinic C2/c structure occupying two different low symmetric and distorted crystallographic sites which would provide strong crystal field for Yb^{3+} ions with quasi-four-level laser operation scheme. SSO crystal retains the highest thermal conductivity among silicate crystals together with the striking negative calorescence coefficient which is crucial for laser operation regarding laser power resistance (Petit, 2005). The crystallographic sites, coordination and mean distance of RE-O in RE_2SiO_5 crystals are extended for ongoing discussion on energy level splitting as shown in Table 2 (Gaume et al., 2003; Ellens et al., 1997).

2.1.1 Lu_2SiO_5

LSO is a positive biaxial crystal with n_Y axis along the b direction and two other axis a and axis c lying in plane (010) (Wang, 2004). The structure of monoclinic LSO crystal with isolated ionic SiO_4 tetrahedral units and non-Si-bonded O atoms in distorted OLu_4 tetrahedron were determined by neutron diffraction (Gustafsson et al., 2001). The OLu_4 tetrahedron form edge-

sharing infinite chains and double O_2Lu_6 tetrahedron along the c axis. The edge-sharing chains are connected to O_2Lu_6 double tetrahedron by isolated SiO_4 units.

Crystal Molecular Formula	LSO	GSO	YSO	SSO	YAG
Space group/simple	C2/c	$P2_1/c$	C2/c	C2/c	Ia3d
Site symmetry	C_1	C_s+C_{3v}	C_1	C_1	D2
Lattice constant (Å)	a=10.2550Å, b=6.6465Å, c=12.3626Å, β=102.422°	a=9.132Å, b=7.063Å, c=6.749Å, β=107.56°	a=10.41Å, b=6.72Å, c=12.49Å, β=102.65°	a=9.961Å, b=6.429Å, c=12.03Å, β=103.8°	a=12.01 Å
Density / g·cm^{-3}	7.4	6.7	4.44	3.52	4.56
Melting point / ℃	2100	1950	2000	1920	1950
Mohs hardness	5.8	5.5	5.6	-	8.5
Thermal conductivity undoped@30℃/W·m^{-1}·K^{-1}	4.9	4.5	4.4	7.5	10.7
dn/dT(*10^{-6} K^{-1})	-	-	7.2	-6.3	7.9
Refractive indices	1.82	1.85	1.782(a) 1.785(b) 1.806(c)	n_x=1.82, n_y=1.84, n_z=1.86	1.83

Table 1. Physicochemical property of monoclinic silicate crystals.

Host	Label	Coordination number	Re^{3+} (Å)	Re–O_{mean} (Å)
LSO	Lu(Ⅰ)	7	1.001	2.277
	Lu(Ⅱ)	6		2.229
GSO	Gd(Ⅰ)	7	1.05	2.49
	Gd(Ⅱ)	9		2.39
YSO	Y(Ⅰ)	7	0.910	2.3080
	Y(Ⅱ)	6		2.2520
SSO	Sc(Ⅰ)	6	0.885	2.2289
	Sc(Ⅱ)	6		2.2149

Table 2. Crystallographic sites, coordination and mean distance in RE-O in RE_2SiO_5 crystal.

2.1.2 Gd_2SiO_5

As seen from Table 1, Gd^{3+} in monoclinic GSO crystal is coordinated with oxygen atoms of 7 and 9, respectively (Fornasiero et al., 1998). The Gd(Ⅰ) coordinated with 7 oxygen is linked with three isolated oxygen ions and three [SiO^{4-}] ions. The Gd(Ⅱ) coordinated with 9 oxygen is bonded with one isolated oxygen and six tetrahedral [SiO^{4-}] ions. As shown in Table 2, the average distance of 2.39 Å in Gd(Ⅰ)–O is shorter than that of 2.49 Å in Gd(Ⅱ)-O (Felsche, 1973) The symmetry and intensity of crystal field would be affected by the coordination field after doping with active Rare Earth ions into the host (Suzuki et al., 1992; Cooke et al., 2000).

2.1.3 Y_2SiO_5

The distorted crystallographic sites of Y^{3+} in YSO crystal are with coordination number of 6 and 7 which is similar to those in LSO. Crystallographic site Y(Ⅰ) forms polyhedron with 5 oxygen from that in tetrahedron $(SiO_4)^{4-}$ and 2 isolated oxygen. Crystallographic site Y(Ⅱ) comprises reticular formation of pseudo octahedron with 4 oxygen from that in tetrahedron $(SiO_4)^{4-}$ and 2 isolated oxygen. The reticular formation of OY_4 is composed of edge-sharing infinite chains along c axis together with the network structure of OSi_4 (IEM Databases and Datasets).

2.1.4 Sc_2SiO_5

The structure of SSO crystal is analogous to those of YSO and LSO, with monoclinic structure and space group of C2/c. Although the large sized Yb:SSO crystal is difficult to obtain due to crystal diameter controlling, the impressive thermo-mechanical properties in SSO crystal make it an excellent performer in high power laser applications (Ivanov, 2001; Gaume et al., 2003; Campos et al., 2004). As indicated in Table 1, SSO crystal possesses a much stronger thermal conductivity of $7.5W \bullet m^{-1} \bullet K^{-1}$ than that in YSO ($4.4W \bullet m^{-1} \bullet K^{-1}$), LSO ($4.5\ W \bullet m^{-1} \bullet K^{-1}$) and GSO ($4.9\ W \bullet m^{-1} \bullet K^{-1}$). Furthermore, SSO crystal preserves the characterization of minus calorescence coefficient dn/dT of $-6.3\times10^{-6}\ K^{-1}$ which is quite different from that of YSO ($7.2\times10^{-6}\ K^{-1}$) and favorable for high power laser operation.

2.2 Crystal growth

Czochralski method (Cz) is one of the major crystal growth methods of obtaining bulk single crystals with high optical quality and fast growth rates from melt for commercial and technological applications. Cz is named after Polish scientist Jan Czochralski, who discovered the method in 1916 while investigating the crystallization rates of metals.

Yb doped silicate crystals such as Yb:LSO, Yb:GSO, Yb:YSO and Yb:SSO studied in this chapter were grown by the Cz method in inductively heated crucibles under inert atmosphere of 5N nitrogen. The starting materials were Rare-Earth Oxide (Lu_2O_3, Gd_2O_3, Y_2O_3 or Sc_2O_3), Yb_2O_3 and SiO_2 powders with purity higher than 99.995%. The powders were mixed and pressed into tablets followed by sintering at 1400℃ for 24 h before loading into the iridium crucible. The chemical reaction is shown in Equation (1). The doping level of Yb ions in the melt was 5at.% with respect to that of Rare-Earth ions in the crystal host. Accordingly the compound formulae of the crystals could be written as $(RE_{0.95}Yb_{0.05})_2SiO_5$.

$$(1-x)RE_2O_3 + SiO_2 + xYb_2O_3 \rightarrow RE_{2(1-x)}Yb_{2x}\ SiO_5 \quad (1)$$

A precisely and oriented rod-mounted seed crystal with diameter of 4.5mm and length of 40mm was introduced for growth. The seeds for Yb:LSO, Yb:YSO, Yb:SSO were oriented along b-axis while that for Yb:GSO crystal was along [100]. The seed crystal was pulled upwards around $0.8\text{-}3mm \cdot h^{-1}$ and rotated simultaneously at 10-30rpm. To keep convex solid–melt interface was important in growing silicate crystals to eliminate engendered dislocations. Temperature gradients and velocity fields were accurately controlled to gain stable settings (Zheng et al., 2007).

Automatic diameter control (ADC) with computer control system and weight sensor or so-called load cell is applied to detect the weight during crystal growth process which is wholesome for increasing crystal yield as well as reducing thermal stress. Strain gauge weight sensor with sufficient resolution was employed comparing with the total weight of

obtained crystals. The input signal of weight sensor via an A/D converter is collected t o calculate the diameter of the generative crystal. A proportional–integral–derivative controller (PID controller) was adopted to better control the loop feedback during temperature regulation.

The difficulty in controlling diameter is originated from encapsulated materials and the high temperature atmosphere which would initiate diameter fluctuation bringing about dislocations besides irregular crystal shape and polycrystallization. The diameter deviation is regulated by controlling the temperature gradients where the double layered zircon cover was designed to optimize the temperature gradients. The heater temperature was increased to reduce the diameter when the measured diameter is larger than expected and vice versa. Crystal boules were finally obtained as shown in Fig. 1.

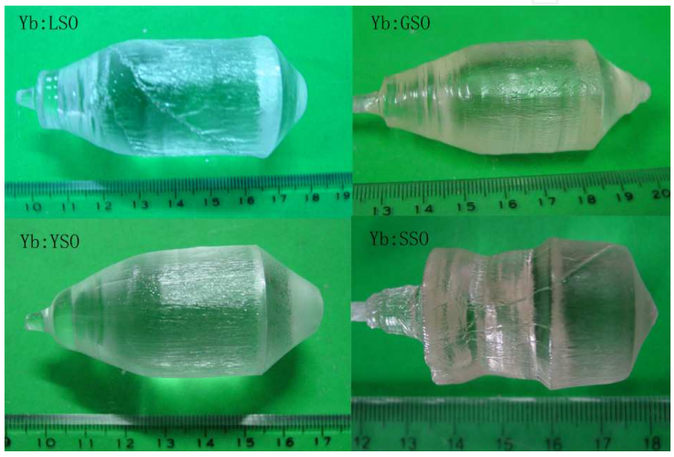

Fig. 1. Bulk crystals of 5at.%Yb doped silicate crystals obtained by Czochralski method.

2.3 Segregation coefficient characterization in silicate crystals

The segregation coefficient of Yb ions in silicate crystal hosts was measured by the inductively coupled plasma atomic emission spectrometer (ICP-AES). Crystal samples adjacent to the seed crystal position were cut and ground into fine powder in an agate mortar. The results of ICP-AES analysis are shown in Table 3.

Sample	seed crystal	Yb^{3+} c_0 (at.%)	Atom content (wt.%)					Yb^{3+} c_{top} (at.%)	k_m
			Yb	Lu	Gd	Y	Sc		
Yb:LSO	LSO	5.0	3.31	70.76	0	0	0	4.515	0.903
Yb:GSO	GSO	5.0	3.06	0	76.22	0	0	3.52	0.704
Yb:YSO	YSO	5.0	5.22	0	0	50.06	0	5.085	1.017
Yb:SSO	SSO	5.0	7.19	0	0	0	36.9	4.82	0.964

Table 3. Segregation coefficients of Yb ions in silicate crystals.

As acquired from Table 3, the segregation coefficient of Yb is 0.903 in Yb:LSO, 0.704 in Yb:GSO, 1.02 in Yb:YSO and 0.964 in Yb:SSO. The solubility of Yb ion in the LSO, YSO and SSO host lattice is higher than that in GSO indicating that Yb ions are liable to incorporate into the crystals with structure of C2/c comparing with that of $P2_1/c$. Meanwhile, the congenial radius of Yb^{3+} (0.868Å) with Lu^{3+}(1.001Å), Y^{3+} (0.910Å) and Sc^{3+} (0.885Å) makes ideal adulteration squaring up that of the Gd^{3+} (1.05Å).

2.4 X-Ray diffraction measurement

The crystal structure of silicate crystals were characterized by powder X-ray diffraction (XRD; Model D/Max 2550V, Rigaku Co., Tokyo, Japan) using Cu Kα radiation (λ = 0.15418 nm). The XRD patterns were inspected using PCPDF software package. Fig. 2 presents the XRD pattern for Yb doped silicate crystals which demonstrated that Yb:LSO, Yb:YSO and Yb:SSO crystals would maintain the primitive monoclinic structure with space group of C2/c, while Yb:GSO maintain that of $P2_1/c$.

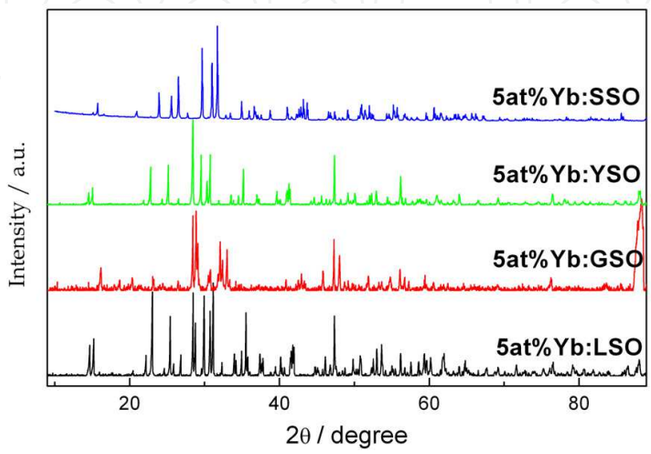

Fig. 2. Comparison of the XRD pattern for Yb doped silicate crystals.

2.5 Absorption and emission spectra

The unpolarized absorption spectra of silicate crystals were measured by JASCO Model V-570 UV/VIS/NIR spectrophotometer at a resolution of 1nm in the range between 860-1100nm with Xe light as pump source.

Fluorescence spectra were measured at a resolution of 1nm from 950nm to 1150nm by TRIAX 550-type spectrophotometer (Jobin-Yvon Company) with 940nm laser pumping source. The fluorescence lifetime with sample thickness of 1mm was pumped with a Xenon lamp and detected with an S-photomultiplier tube, while the data of emission decay curve was collected by a computer-controlled transient digitizer simultaneously.

2.6 Laser experiment

Kerr-lens mode-locked is well-developed for ultrafast pulses in efficient and compact lasers which is initiated by the self-focusing effect yielded from the nonlinear refractive-index variation in laser crystal. Diode-pumped mode-locked Yb:LSO laser with a W-typed cavity was developed based on Kerr-lens effect. The experimental setup for mode-locked Yb:LSO lasers was represented in Fig. 3. The maximum output power of the fiber-coupled diode-pumped semiconductor laser reached 30W around the emitting wavelength of 978 nm. The radius and the numerical aperture of the fiber were with 200 μm and 0.22, respectively. Yb:LSO host was cut into the dimension of 3×3×2 mm^3 and end-coated with antireflection at lasing wavelength of 1030-1080 nm and pump wavelength of 978 nm. Yb:LSO wrapped with indium foil was placed with a small angle to suppress the Fabry-perot etalon effect and mounted in a water-cooled copper block with temperature maintained at 14 ℃.

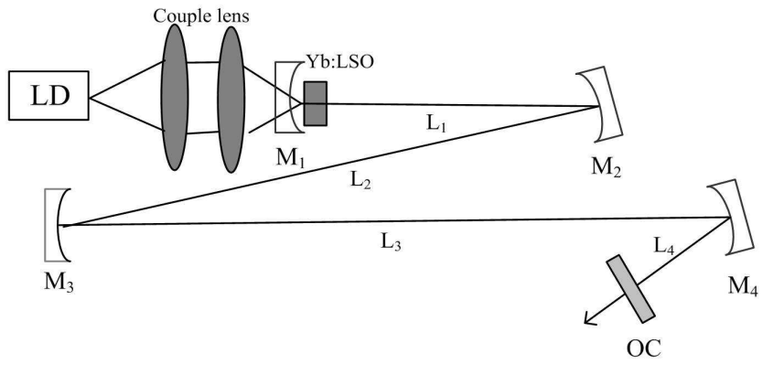

Fig. 3. Schematic of the Kerr-lens Yb: LSO laser.

Laser experiments on Yb:GSO crystal was performed with aperture of 5×6 mm² and length of 5 mm. The crystal was end pumped by a 30 W fiber-coupled laser diode with emission centered at 974 nm. The diameter and numerical aperture of the fiber core were 400 μm and 0.22, respectively. The laser cavity consisted of two mirrors M1 and output coupler OC, where dichroic mirror M1 was with anti-reflection coating at 974 nm and high-reflection coating in a broadband of 1020-1120 nm besides OC with various transmission.
The schematic of the Yb:SSO laser is shown in Fig. 4. The b-cut Yb:SSO crystal is with dimensions of 2.2 × 3 × 3 mm³. The crystal was coated at both the pump and laser wavelengths with high transmission coatings to minimize the Fresnel reflection losses. The crystal was titled to about 6° with respect to the principle axis of the cavity to suppress etalon effects and improve the stability of the mode-locking operation. A single emitter diode with central wavelength at (975 ± 3) nm was used as the pump source.

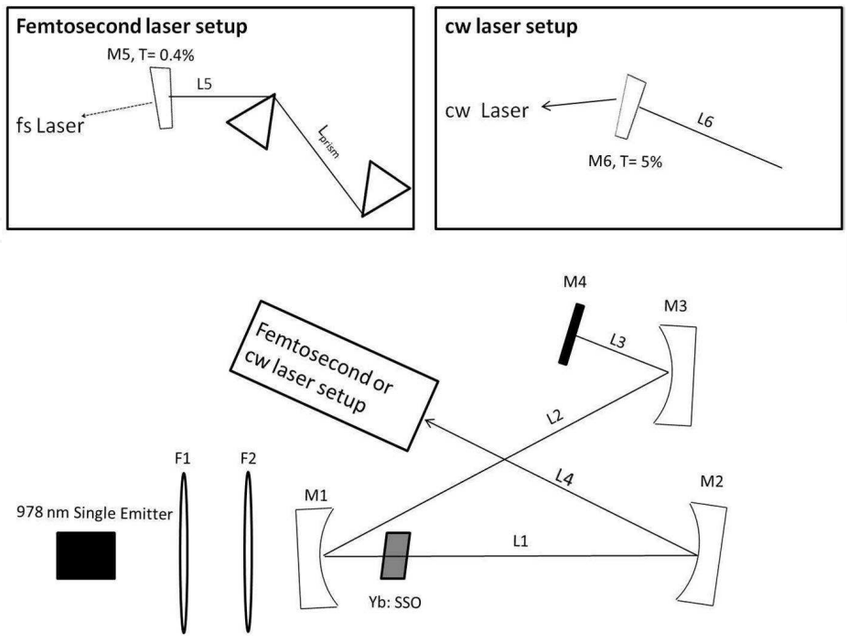

Fig. 4. Schematic of the experimental setup for Yb:SSO laser.

3. Spectra analysis of silicate crystals

Absorption and fluorescence spectra in Yb doped silicate crystals were presented. Based on the above spectra, key parameters were calculated for predicting the laser performance of the studied hosts.

3.1 Absorption and fluorescence spectra

Fig. 5 showed the absorption spectra of Yb doped silicate crystals with main absorption peak located around 920nm and 978 nm which is suitable for InGaAs diode pump.
The absorption bands were corresponding to the typical transitions from ground state $^2F_{7/2}$ to the sublevels of $^2F_{5/2}$. The absorption peak around 978nm belongs to the zero-line transition between the lowest sublevels of $^2F_{7/2}$ and $^2F_{5/2}$ manifolds. Broad absorption bands are beneficial for enhancing the efficiency of diode-pump operation since the laser diodes are typically emitting at a wide spectral range of 5 nm and presenting a thermal shift at the peak wavelength. As manifested in Fig. 5, the broad fluorescence behavior was associated with the typical transitions from the lowest level of $^2F_{5/2}$ to the sublevels of $^2F_{7/2}$ manifold. The emission band above 1080nm was due to transition from the lowest levels of $^2F_{5/2}$ manifold to the highest levels of $^2F_{7/2}$ manifold.

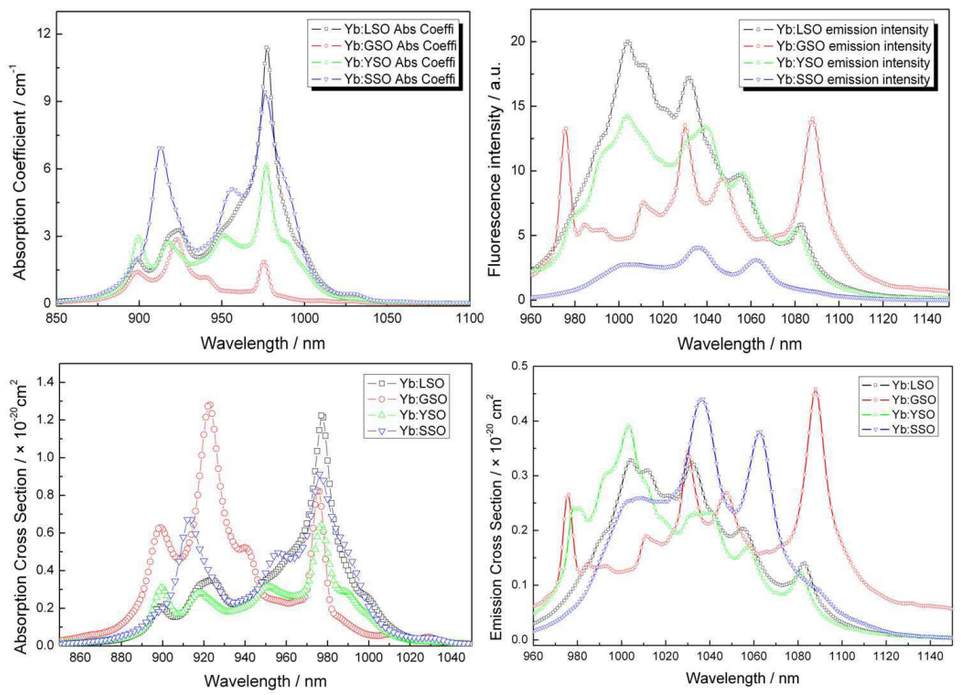

Fig. 5. Absorption coefficients, Fluorescence Intensity, Absorption cross section and emission cross section of Yb doped silicate crystals.

$$\sigma_{abs} = \frac{\alpha}{N} \tag{2}$$

$$\sigma_{em}(\lambda) = \frac{\lambda^5 I(\lambda)}{8\pi n^2 c \tau_{rad} \int \lambda I(\lambda) d\lambda} \tag{3}$$

Parameter	5 at. % Yb:LSO	5 at. % Yb:GSO
Main absorption peaks λ_{abs} (nm)	899, 924, 977	897, 922, 940, 976
Absorption bandwidth (nm)	13, 25, 15	17, 26, 24, 10
Absorption cross-section σ_{abs}(10^{-20} cm^2)	0.21, 0.36, 1.3	0.33, 0.60, 0.39, 0.51
Fluorescence peak (nm)	1004, 1012, 1032,1055, 1083	976, 1011, 1030, 1047, 1088
Emission cross-section σ_{em} (10^{-20} cm^2)	0.34, 0.32, 0.33, 0.21, 0.14	0.17, 0.45, 0.31, 0.46
Emission bandwidth (nm)	73	72
Fluorescence lifetime (ms)	1.68 @ 1083nm	1.56 @ 1088nm
Parameter	5 at. % Yb:YSO	5 at. % Yb:SSO
Main absorption peaks λ_{abs} (nm)	899, 917, 950, 977	914, 956, 976
Absorption bandwidth (nm)	15, 24, 31, 13	18, 19, 24
Absorption cross-section σ_{abs}(10^{-20} cm^2)	0.31, 0.28, 0.32, 0.64	0.67, 0.49, 0.91
Fluorescence peak (nm)	980, 1003, 1040, 1056, 1081	1006, 1036, 1062, 1087
Emission cross-section σ_{em} (10^{-20} cm^2)	0.24, 0.39, 0.23, 0.18, 0.12	0.26, 0.44, 0.38, 0.1
Emission bandwidth (nm)	48	57
Fluorescence lifetime (ms)	1.74 @ 1081nm	1.64 @ 1035nm

Table 4. Spectroscopic parameters of Yb doped silicate crystals.

Fig. 5 also revealed the calculated σ_{abs} of Yb^{3+} according to Equation (2) where α means the absorption coefficient and *N* presents the concentration of Yb^{3+} ions. σ_{em} of Yb^{3+} in silicate hosts explicated in Fig. 5 were calculated by Füchtbauer-Ladenburg formula referring to Equation (3) where τ_{rad} stands for the radiative lifetime of the excited manifold $^2F_{5/2}$ of Yb^{3+}, I(λ) for the emission intensity at wavelength λ, n for refractive index and c for light velocity (Caird et al., 1991; Deloach et al., 1993). σ_{em} is fit for describing available gain at given inversion density. The lifetime of excited manifold $^2F_{5/2}$ was measured to be 1.68ms, 1.56ms, 1.74ms and 1.64ms in Yb:LSO, Yb:GSO, Yb:YSO and Yb:SSO crystals respectively. The lifetime is much longer than that of 0.8ms in Yb:YAG. Table 4 outlined the spectroscopic parameters of Yb^{3+} in silicate hosts based on absorption and emission spectra.

The large overlapping between absorption and emission spectra was observed in Fig. 5 due to the transitions among the multiplets of $^2F_{7/2}$ and $^2F_{5/2}$ manifolds of Yb^{3+}. The emission bandwidth FWHM of Yb:LSO crystal is appropriately 73nm which is much larger than that of Yb:YSO and Yb:GSO crystal. Although Yb:LSO possessed the largest σ_{em} around 1004nm,

the reabsorption losses was consequently strong which would detrimentally affect laser action. σ_{em} of the terminal laser level at 1083nm was with 1.4×10^{-21} cm^2 containing the smallest thermal populating as well as the least re-absorption losses. In the case of 1032nm, the emission cross section is large enough to obtain low threshold and high efficient laser operation.

The absorption spectrum in Yb:GSO crystal was mainly composed of four strong bands centered at 897 nm, 922 nm, 940 nm and 976 nm. σ_{abs} at 922 nm and 976 nm were estimated as 6.0×10^{-21} and 5.1×10^{-21}, cm^2 with the absorption bandwidths of 26 nm and 10 nm, respectively. The emission spectrum mainly included four bands centered at 1011 nm, 1030 nm, 1047 nm and 1088 nm with fluorescence lifetime of 1.56 ms at 1088 nm which would be treated as radiative lifetime since the re-absorption loss could be negligible at 1088 nm. The σem at 1088 nm were 4.2×10^{-21} which was with the strongest cross section as well as the lowest pumping threshold. Referring to the spectra in Yb:YSO crystal, the strongest absorption peak was located at 978nm with furthest and weakest emission band centered at 1080 nm. The strongest σem centered at 1003 nm was severely affected by strong re-absorption losses. Yb^{3+} ions in Yb:SSO crystal show an inhomogeneous broad absorption band with peak absorption coefficient of $9.43cm^{-1}$ at 976nm which is higher than that in Yb:GSO crystal. The furthest σem centered at 1087 nm was with 1.0×10^{-21}, cm^2 in Yb:SSO which was at the same level of that in Yb:LSO and Yb:YSO. In conclusion, Yb:SSO with wide spectra bandwidth and long lifetime is favorable for high-efficiency ultra-fast diode-pump lasers.

3.2 Gain cross-section σ_g and minimum pump intensity I_{min}

The pump threshold and energy extraction would affect the application of Yb doped crystals on laser devices. Gain cross section σ_g was calculated according to Equation (4) to predict the laser performance (Deloach et al., 1993).

$$\sigma_g = \beta\,\sigma_{em} - (1-\beta)\,\sigma_{abs} \tag{4}$$

$$I_{sat}=h\upsilon/(\sigma_{abs}\cdot\tau_{em}) \tag{5}$$

The inversion coefficient β is defined as the population ratio on the $^2F_{5/2}$ level over the total Yb^{3+} ions population density. σ_g is equal to the emission cross-section σ_{em} when β is equal to 1. To effectively assemble the diode-pumped Yb-laser systems, a substantial fraction of Yb ions on the ground state should be driven to the excited state in order to achieve adequate gain and to overwhelm the absorption losses. As indicated in Equation (5), Pump saturation intensity I_{sat} would be reduced along with stronger σ_{abs} and longer emission life time τ_{em}. The excitation fraction of Yb ions is given by I_{abs}/I_{sat} where I_{abs} stands for the absorbed pump power. Long τ_{em} would promote accumulation of population inversion at fixed power as a complement of the peak-power-limited InGaAs diode sources.

The minimum excitation fraction β_{min} of Yb^{3+} ions calculated by Equation (6) must be balanced for laser output (Moulton, 1983). The parameter of minimum pump intensity I_{min}, obtained by Equation (7), represents the minimum pumping intensity required to invert population in a quasi-three-level system. The fraction I_{abs}/I_{sat} of excited Yb ions equalling to the required fractional excitation of β_{min} permits the equation of I_{min} and I_{abs}. Hence, I_{min} may be interpreted as the absorbed pump intensity required to surpass threshold in a lossless oscillator or to balance at selected extraction wavelength λ_{ext} in amplifier configuration.

$$\beta_{\min} = \frac{\sigma_{abs}(\lambda_{ext})}{\sigma_{ext}(\lambda_{ext}) + \sigma_{abs}(\lambda_{ext})} \tag{6}$$

$$I_{min}=\beta_{min}\cdot I_{sat} \tag{7}$$

Key spectroscopic parameters are interpreted for designing high power rare-earth lasers. Strong σ_{abs} permits low Yb^{3+} ion doping level which in turn leads to a lower resonance absorption loss and a higher small-signal gain at given pump flux. I_{min} was accounted as a figure-of-merit to evaluate the potential Yb doped gain media for laser application by describing the suitable inversion density. Altogerther, I_{sat} as well as the minimum pump intensities I_{min} would be deduced from the absorption cross sections σ_{abs}.

3.2.1 Spectra parameters on Yb: LSO crystal

Fig. 6 showed the gain cross-section with various inversion ratio β. The emission spectra extending from 1000nm to 1092nm at β values of 0.5 was beneficial to laser output. The minimum pump intensities I_{min} at the selected extraction wavelengths, as well as the saturable pump density I_{sat} and the β_{min} under different laser output were also presented.

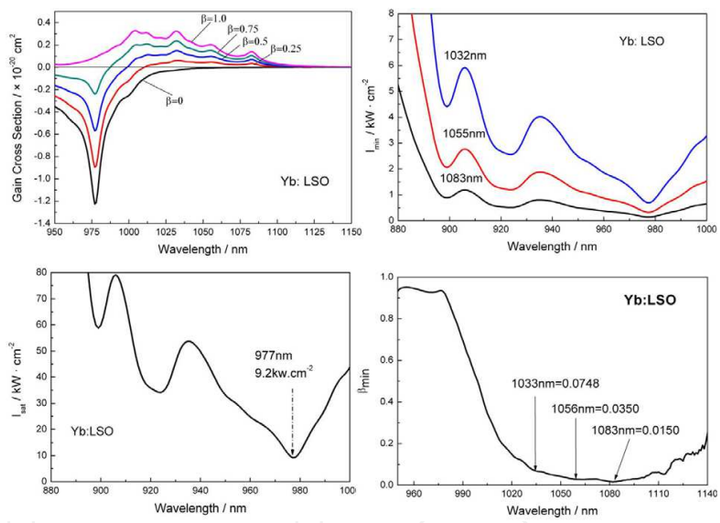

Fig. 6. σ_g, I_{min}, I_{sat} and β_{min} in Yb:LSO crystal.

3.2.2 Spectra parameters on Yb: GSO crystal

Fig. 7 presented the gain cross section σ_g of Yb:GSO crystal at β values of 0, 0.25, 0.5, 0.75 and 1. The emission spectra extending from 999nm to 1150nm at β values of 0.5 was beneficial to ultra-short pulse laser output. The minimum pump intensities I_{min} of 1.9kW/cm², 0.71kW/cm² and 0.094kW/cm² were achieved for selected extraction wavelengths at 1030nm, 1048nm and 1088nm as shown in Fig. 7.

The pump threshold power at the furthest wavelength of 1088nm was much lower than that of 0.13kW/cm² at 1083nm in Yb:LSO crystal which predicted low threshold and high efficient laser output in Yb:GSO crystal. Fig. 7 indicated the saturable pump density I_{sat}. The β_{min} at various laser output wavelength in Yb:GSO crystal was shown in Fig. 7 and the comparatively lowest was located at 1088nm with the β_{min} value of 0.0071 which was half less than that of 0.015 at 1082nm in Yb:LSO crystal.

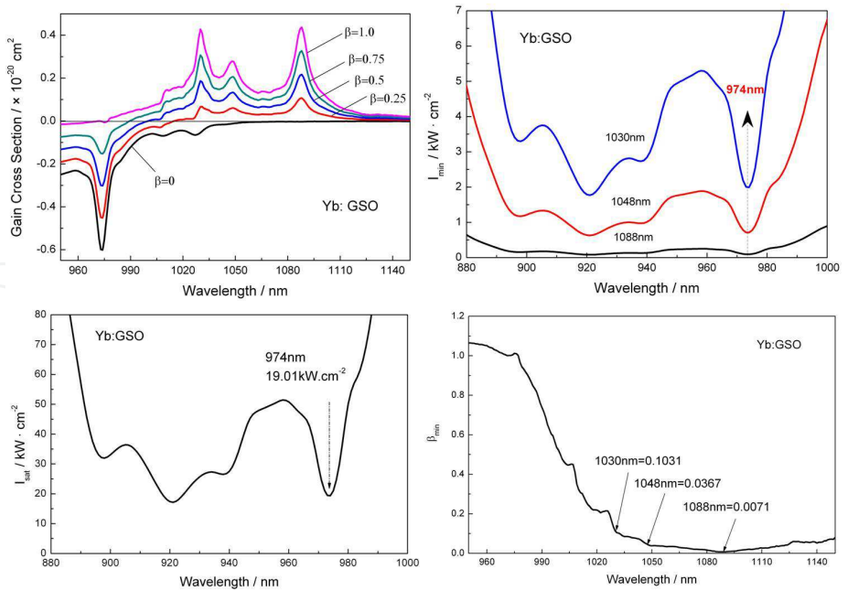

Fig. 7. σ_g, I_{min}, I_{sat} and β_{min} in Yb:GSO crystal.

3.2.3 Spectra parameters on Yb: YSO crystal

Fig. 8 presented the gain cross section of Yb:YSO crystal at β values of 0-1. The emission spectra stretched from 990nm to 1100nm at β values of 0.5. The minimum pump intensities I_{min} of 1.38kW/cm², 0.52kW/cm² and 0.2kW/cm² were achieved for selected extraction wavelengths at 1035nm, 1056nm and 1081nm as shown in Fig. 8. Fig. 8 indicated the saturable pump density I_{sat} in Yb:YSO crystal as well as the β_{min} at various laser output wavelength. The lowest β_{min} was located at 1081nm with the value of 0.015 which was almost the same as that in Yb:LSO crystal.

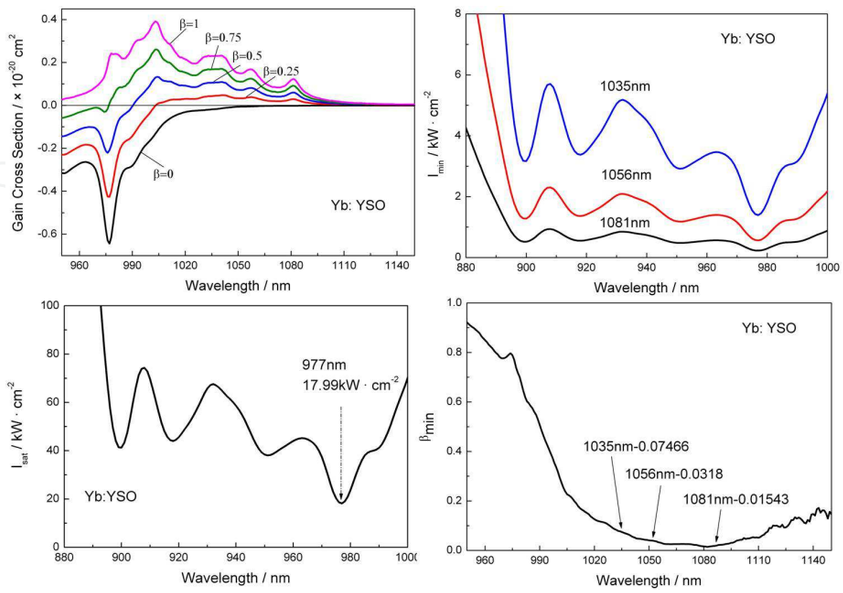

Fig. 8. σ_g, I_{min}, I_{sat} and β_{min} in Yb:YSO crystal.

3.2.4 Spectra parameters on Yb: SSO crystal

Fig. 9 presented the gain cross section of Yb:SSO crystal at β values of 0-1. The emission spectra elongated from 990nm to 1120nm at β values of 0.5. The minimum pump intensities I_{min} of 0.261kW/cm², 0.077kW/cm² and 0.2033kW/cm² were achieved for selected extraction wavelengths at 10356nm, 1062nm and 1087nm as shown in Fig. 9.

Fig. 9 indicated the saturable pump density I_{sat} in Yb:SSO crystal. The β_{min} at various laser output wavelength in Yb:SSO crystal was shown in Fig. 9. The lowest β_{min} was located at 1087nm with the value of 0.007148 which was almost half of that in Yb:LSO crystal. As concluded in Table 5, the laser parameters of Yb doped silicate crystals were listed and compared with that of Yb:YAG crystal (Haumesser et al., 2002).

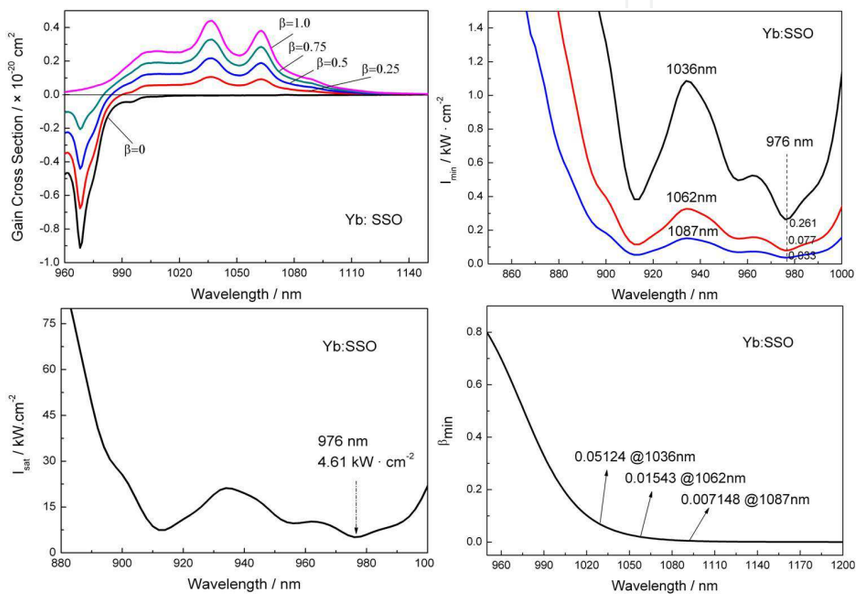

Fig. 9. σ_g, I_{min}, I_{sat} and β_{min} in Yb:SSO crystal.

Host	λ_{pump} (nm)	β_{min}	I_{sat} (kW/cm²)	I_{min} (kW/cm²)	λ_{ext} (nm)	σ_{ext} (10^{-20}cm²)
Yb:LSO	977	0.015	9.2	0.138	1083	0.14
Yb:GSO	974	0.0071	19.01	0.093	1088	0.46
Yb:YSO	977	0.0015	17.99	0.18	1081	0.12
Yb:SSO	976	0.0071	4.61	0.033	1087	0.1
Yb:YAG	942	0.055	28.8	1.53	1030	2.2

Table 5. Calculated Laser parameters of Yb doped Crystals.

3.3 Energy level of Yb in silicate crystal hosts

The energy level schemes for Yb doped silicate crystals were determined by optical spectroscopic analysis and semi-empirical crystal-field calculations using the simple overlap model. The stark levels distributed in the two $^2F_{7/2}$ and $^2F_{5/2}$ manifolds are labeled from one to four in the ground state and five to seven in the excited state. The maximum splitting manifolds of Yb in silicate hosts was calculated according to the spectra shown in Fig. 5.

Fig. 10 explicated the overall energy splitting of $^2F_{7/2}$ manifold of Yb^{3+} in silicate crystal hosts with 1012cm^{-1} in Yb:LSO crystal, 1076cm^{-1} in Yb:GSO crystal, 984 cm^{-1} in Yb:YSO crystal and 1027cm^{-1} in Yb:SSO crystal indicating much stronger crystal-field interaction in silicate hosts than that in Yb:YAG with energy splitting of 785cm^{-1} (Yan et al., 2006).

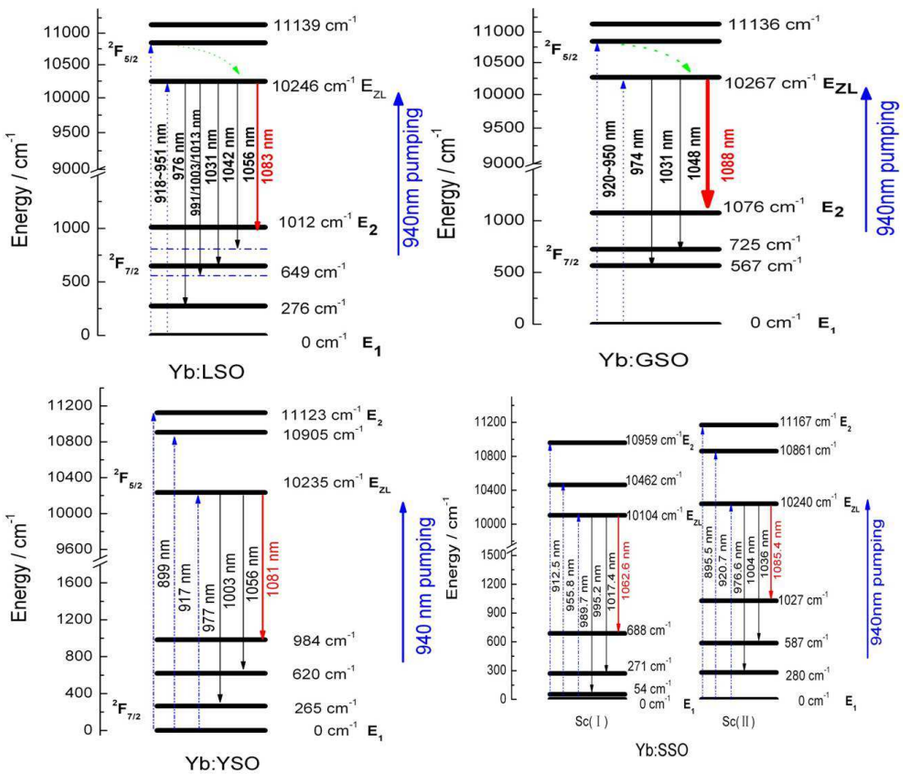

Fig. 10. Energy level of Yb^{3+} in Yb doped silicates.

As indicated in Fig. 10, the manifold splitting for Yb^{3+} in Yb:GSO crystal reached 1076 cm^{-1} which was much larger than that in Yb:LSO, Yb:YSO and Yb:SSO with C2/c structure thanks to the anisotropic and compact structure in GSO crystal. The strong crystal field in Yb:GSO crystal was simultaneously the largest ground-state splitting among Yb doped silicate crystals as obtained by absorption spectra starting from around 897 nm and the emission spectra extending till 1090 nm in Yb:GSO host.

To further elaborate the energy level in Yb doped silicate crystals, we found that the absorption band centered at 976nm in Yb:GSO belongs to the zero-line transition between the lowest level of $^2F_{7/2}$ and $^2F_{5/2}$ manifolds. The emission band at the longest wavelength around 1088 nm corresponds to the transition from the lowest levels of $^2F_{5/2}$ manifold to the highest levels of $^2F_{7/2}$ manifold. The strong electron–phonon coupling among Yb^{3+} ions together with the considerable interaction between Yb^{3+} ions and lattice vibrations give arise to strong vibration sidebands. The supplementary stark level splitting was incited by the resonance between stark levels and phonons which can be easily mistaken for the assignment of electronic transitions. Large crystal-field splitting of the fundamental manifold $^2F_{7/2}$ is critical for limiting the thermal population of the terminal laser level. In other words, less thermal populating of the terminal laser level of $^2F_{7/2}$ ground state would

reduce re-absorption losses and decrease laser threshold as well. The strongest emission cross section was around 1000 nm in either Yb:YSO or Yb:LSO, while that in Yb:GSO was located around 1088 nm suggesting weakest re-absorption losses and least thermal populating of the terminal laser level. Accordingly, Yb:GSO around 1088 nm would produce ultra-fast laser with lowest pumping threshold.

The energy-level diagram of Yb^{3+} ions in crystallographic site Sc(Ⅰ) and crystallographic site Sc(Ⅱ) located in Yb:SSO crystal was approximately denoted in Fig. 10. The overall splitting of the $^2F_{7/2}$ manifold of Sc(Ⅱ) reached about 1027cm^{-1} which was approaching that in Yb:GSO but much larger than 984 cm^{-1} in Yb:YSO and 1012 cm^{-1} in Yb:LSO. Yb ions encountered a stronger crystal-field interaction in SSO host indicating that Yb:SSO crystal would be the suitable solid-state laser gain for high efficient and high power application.

4. Laser peformance of Yb doped silicate crystals

High efficient laser output of 198fs/2.61W, 260fs/2.6W and 343fs/400mW were obtained in Yb:YSO, Yb:LSO and Yb:GSO respectively by Chinese and French researchers (Thibault et al., 2006; Li et al., 2007). Based on laser setup in Fig. 3, diode-pumped Kerr-lens mode-locked Yb:LSO laser was achieved without additional components. The mode-locked laser pulses were obtained in five-mirror cavity with average output power of 2.98 W and repetition rate of 103 MHz under incident pump power of 14.44W. Short pulse of 8.2 ps was realized at wavelength centered at 1059 nm (Wang et al., 2010). With an OC of T=2.5%, the cw Yb:GSO lasers with the slope efficiency of 75% at 1094 nm were achieved. Self-pulsed Yb:GSO lasers were achieved with low pumping threshold from 1091nm to 1105 nm (Li et al., 2006). Efficient diode-pumped laser performance of Yb:SSO was demonstrated with slope efficiency of 45% and output power of 3.55W (Zheng et al., 2008). The passive mode-locking and cw lasing performance of Yb:SSO was carried out in an x-fold cavity end-pumped by a 978 nm single emitter. The laser produced a maximum cw output power of 2.73 W with a slope efficiency of 70%. Preliminary tests regarding the laser operation of the thin-disk Yb:SSO laser were presented with 9.4 W of output power with an optical efficiency of 25.3 % (Wentsch et al., 2011). Passive mode-locking of Yb: SSO was initiated using a semiconductor saturable absorber mirror (SESAM) while dispersion compensation was introduced using a pair of SF10 prisms. The laser mode-locked at 1041 nm, 1060 nm and 1077 nm with near Fourier transformed limited pulse width of 145 fs, 144 fs and 125 fs, and average output power of 40 mW, 52 mW and 102 mW, respectively (Tan et al., 2010).

5. Conclusion

Yb doped oxyorthosilicate single crystals as technologically important laser host family owing to quasi-four level scheme were successfully obtained with high transparency and high quality by Czmethod. The efficient diode pumped ultra-fast laser was achieved with distinguished ground-state splitting up to 1000 cm^{-1}. Key spectroscopic parameters of Gain cross-section σ_g and minimum pump intensity I_{min} for designing high power lasers are specifically interpreted. In future, bulk silicate crystals with favorable thermal properties and multi-crystallographic sites for introducing distorted and broad spectra behavior are among the hot spots in the development of ultra-fast lasers.

6. Acknowledgment

The authors thank the supports from National High Technology Research and Development Program of China(2009AA03Z435), National Natural Science Foundation of China (60938001, 60908030, 61178056, 61177037), Innovation Project of Shanghai Institute of Ceramics (Y04ZC5150G), Hundred Talents Project of Chinese Academy of Sciences and National Science Fund for Distinguished Young Scholars. Special thanks to Dr. Heping Zeng, Dr. Xiaoyan Liang, Dr. Jie Liu, Dr. Weide Tan ,Dr. Guangjun Zhao, Dr. Chengfeng, Yan, Dr. Kejian Yang, Dr. Nengyin Sheng, Ms. Jiao Wang.

7. References

Caird J., Ramponi A. & Staver P. (1991). Quantum efficiency and excited-state relaxation dynamics in neodymium-doped phosphate laser glasses. *Journal of the Optical Society of America B*, Vol.8, No.7, pp. 1391-1403, ISSN 0740-3224

Camargo A., Davolos M. & Nunes L. (2002). Spectroscopic characteristics of Er^{3+} in the two crystallographic sites of Gd_2SiO_5, *Journal of Physics: Condensed Matter*, Vol.14, No.12, pp. 3353-3363, ISSN 0953-8984 (print)

Campos S., Denoyer A., Jandl S., Viana B., Vivien D., Loiseau P. & Ferrand B. (2004). Spectroscopic studies of Yb^{3+}-doped rare earth orthosilicate crystals. *Journal of Physics: Condensed Matter*, Vol.16, No.25 pp. 4579-4590, ISSN 0953-8984 (Print)

Cooke D., Bennett B., Mcclellan K., Roper J., Whittaker M. (2000). Oscillator strengths, Huang-Rhys parameters, and vibrational quantum energies of cerium-doped gadolinium oxyorthosilicate. Journal of Applied Physics, Vol.87, No.11, pp. 7793-7797, ISSN 0021-8979 (Print)

Deloach L., Payne S., Chase L., Smith L., Kway W. & Krupke W. (1993). Evaluation of absorption and emission properties of Yb^{3+} doped crystals for laser applications. *IEEE Journal of Quantum Electronics*, Vol.29, No.4, pp. 1179 - 1191, ISSN 0018-9197

Du J., Liang X., Xu Y., Li R., Xu Z., Yan C., Zhao G., Su L. & Xu J. (2006). Tunable and efficient diode-pumped Yb^{3+}:GYSO laser. *Optics Express*, Vol.14, No.8, pp. 3333-3338, ISSN 1094-4087

Eijk C. (2001). Inorganic-scintillator development. *Nuclear Instruments and Methods in Physics Research Section A*, Vol.460, No.1, pp. 1-14, ISSN 0168-9002

Ellens A., Andres H., Meijerink A. & Blasse G. (1997). Spectral-line-broadening study of the trivalent lanthanide-ion series.I. Line broadening as a probe of the electron-phonon coupling strength. *Physical Review B*, Vol.55, No.1, pp. 173-179, ISSN 1098-0121

Felsche J., (1973). The crystal chemistry of the rare-earth silicates, *Structure and Bonding*, pp. 99-197, ISSN 0081-5993 (Print), Springer-Verlag, New York, 1973

Fornasiero L., Petermann K., Heumann E. & Huber G. (1998). Spectroscopic properties and laser emission of Er^{3+} in scandium silicates near 1.5 μm, *Optical Materials*, Vol.10, No.1, pp. 9-17, ISSN 0925-3467

Gaume M. (2002). Relations structures - propriétés dans les lasers solides de puissance à l'ytterbium. Elaboration et caractérisation de nouveaux matériaux et de cristaux composites soudés par diffusion, These De Doctorat de l'universite pierre et marie curie-paris VI

Gaume R., Viana B., Derouet J. & Vivien D. (2003). Spectroscopic properties of Yb-doped scandium based compounds Yb:$CaSc_2O_4$, Yb:$SrSc_2O_4$ and Yb:Sc_2SiO_5. *Optical Materials*, Vol.22, No.2, pp. 107-115, ISSN 0925-3467

Giesen A. & Speiser J. (2007). Fifteen Years of Work on Thin-Disk Lasers: Results and Scaling Laws. *IEEE Journal of Selected Topics in Quantum Electron*, Vol.13, No.3, pp.598-609, ISSN 1077-260X

Griebner U., Petrov V., Petermann K. & Peters V. (2004). Passively mode-locked Yb:Lu_2O_3 laser. *Optics Express*, Vol.12, No.14, pp. 3125-3130, ISSN 1094-4087

Gustafsson T., Klintenberg M., Derenzo S., Weber M., Thomas J. (2001). Lu_2SiO_5 by single-crystal X-ray and neutron diffraction. *Acta Crystallographica Section C*, Vol.57, No.6, pp. 668-669, ISSN 1600-5759 (Online)

Haumesser P., Gaumé R., Viana B. & Vivien D. (2002). Determination of laser parameters of ytterbium-doped oxide crystalline materials. *Journal of the Optical Society of America B*, Vol.19, No.10, pp. 2365-2375. ISSN 0740-3224

http://database.iem.ac.ru/

Ivanov V., Petrov V., Pustovarov V., Shulgin B., Vorobjov V., Zinevich E., Zinin E., (2001). Electronic excitations and energy transfer in A_2SiO_5–Ce (A=Y, Lu, Gd) and Sc_2SiO_5 single crystals, *Nuclear Instruments and Methods in Physics Research Section A*, Vol.470, No.1-2, pp. 358-362, ISSN 0168-9002

Keller U. (2003). Recent developments in compact ultrafast lasers. *Nature*, Vol.424, No.6950, pp. 831-838, ISSN 0028-0836

Kisel V., Troshin A., Shcherbitsky V., Kuleshov N., Matrosov V., Matrosova T., Kupchenko M., Brunner F., Paschotta R., Morier-Genoud F. & Keller U. (2005). Femtosecond pulse generation with a diodepumped Yb^{3+}:YVO_4 laser. *Optics Letters*, Vol.30, No.10, pp. 1150-1152, ISSN 0146-9592

Krupke W. (2000). Ytterbium solid-state lasers-the first decade. *IEEE Journal of Selected Topics in Quantum Electron*, Vol.6, No.6, pp. 1287-1296, ISSN 1077-260X

Kuleshov N., Shcherbitsky V., Lagatsky A., Mikhailov V., Minkov B., Danger T., Sandrock T. & Huber G. (1997). Spectroscopy, excited-state absorption and stimulated emission in Pr^{3+}-doped Gd_2SiO_5 and Y_2SiO_5 crystals. Journal of Luminescence, Vol.71, No.1, pp. 27-35, ISSN 0022-2313

Lacovara, P., Choi, H., Wang, C., Aggarwal, R. & Fan T. (1991). Room-temperature diode-pumped Yb:YAG laser. *Optics Letters*, Vol.16, No.14, 1089-1091, ISSN 0146-9592 (print)

Li W., Hao Q., Zhai H., Zeng H., Lu W., Zhao G., Zheng L., Su L. & Xu J. (2007). Diode-pumped Yb:GSO femtosecond laser. *Optics Express*, Vol.15, No.5, pp. 2354-2359, ISSN 1094-4087

Li W., Pan H., Ding L., Zeng H., Lu W., Zhao G., Yan C., Su L. & Xu J. (2006). Efficient diode-pumped Yb:Gd_2SiO_5 laser. *Applied Physics Letters*, Vol.88, No.22, pp. 221117(1-3), ISSN 0003-6951 (Print)

Liu H., Nees J. & Mourou G. (2001). Diode-pumped Kerr-lens mode-locked Yb:$KY(WO_4)_2$ laser. *Optics Letters*, Vol.26, No.21, pp. 1723-1725, ISSN 0146-9592

Melcher C. & Schweitzer J. (1992). Cerium-doped lutetium oxyorthsilicate: A fast, efficient new scintillator, *IEEE Transactions on Nuclear Science*, Vol.39, No.4, pp. 502-505, ISSN 0018-9499

Moulton P. (1983). Paramagnetic ion lasers, in: *Handbook of Laser Science and Technology*, M.J. Weber, (Ed.), CRC, ISBN: 978-0-8493-3508-2 , Boca Raton, FL

Pelenc D., Chambaz B., Chartier I., Ferrand B., Wyon C., Shepherd D., Hanna D., Large A. & Tropper A. (1995). High slope efficiency and low threshold in a diode-pumped epitaxially grown Yb:YAG waveguide laser. *Optics Communication*, Vol.115, No.5-6, pp. 491-497, ISSN 0030-4018

Petit J., Goldner P. & Viana B. (2005). Laser emission with low quantum defect in Yb:$CaGdAlO_4$. *Optics Letters*, Vol.30, No.11, pp. 1345-1347, ISSN 0146-9592

Smolin Y. & Tkachev S. (1969). Determination of the structure of gadolinium oxyorthosilicate (Gd_2SiO_5). *Kristallografiya*, Vol.14, pp.22, ISSN 0023-4761

Su L., Xu J., Li H., Yang W., Zhao Z., Si J., Dong Y. & Zhou G. (2005). Codoping Na^+ to modulate the spectroscopy and photo-luminescence properties of Yb^{3+} in CaF_2 laser crystal. *Optics Letters*, Vol.30, No.9, pp. 1003-1005, ISSN 0146-9592

Suzuki H., Tombrello T., Melcher C. & Schweitzer J. (1992). UV and gamma-ray excited luminescence of cerium-doped rare-earth oxyorthosilicate. *Nuclear Instruments and Methods in Physics Research Section A*, Vol.320, No.1-2, pp. 263-272, ISSN 0168-9002

Tan W., Tang D., Xu X., Zhang J., Xu C., Xu F., Zheng L., Su L. & Xu J. (2010). Passive femtosecond mode-locking and cw laser performance of Yb^{3+}:Sc_2SiO_5. *Optics Express*, Vol.18, No.16, pp. 16739-16744, ISSN 1094-4087

Thibault F., Pelenc D., Druon F., Zaouter Y., Jacquemet M. & Georges P. (2006). Efficient diode-pumped Yb^{3+}:Y_2SiO_5 and Yb^{3+}:Lu_2SiO_5 high-power femtosecond laser operation. *Optics Letters*, Vol.31, No.10, pp. 1555-1557, ISSN 0146-9592

Uemura S. & Torizuka K. (2005). Center-wavelength-shifted passively mode-locked diode-pumped ytterbium (Yb):Yttrium aluminum garnet (YAG) laser. *Jpn. J. Appl. Phys.*, Vol.44, No.12-15, pp. L361-L363, ISSN: 0021-8979 (print)

Wang W., Liu J., Chen W., Lu C., Zheng L., Su L., Xu J. & Wang Y. (2010). Diode-Pumped Passively Mode-Locked Yb:LSO/SESAM Laser. *Laser Physics*, Vol.20, No.4, pp. 740-744, ISSN 1054-660X (Print)

Wang X., (2004). *Optical Crystallography*, Nanjing University Press, ISSN 7-305-04088-6

Wentsch K., Weichelt B., Zheng L., Xu J., Abdou-Ahmed M. & Graf T. (2011) Contnious-wave Yb doped Sc_2SiO_5 thin-disk laser. *Optics Letters*, Vol. Accepted 11/08/2011, Doc. ID 153527, ISSN 0146-9592

Yan C., Zhao G., Su L., Xu X., Zhang L. & Xu J. (2006). Growth and spectroscopic characteristics of Yb:GSO single crystal. *Journal of Physics: Condensed Matter*, Vol.18, No.4, pp. 1325-1333, ISSN 0953-8984 (Print)

Zheng L., Xu J., Zhao G., Su L., Wu F., Liang X. (2008). Bulk crystal growth and efficient diode-pumped laser performance of Yb^{3+}:Sc_2SiO_5. *Applied Physics B*, Vol.91, No.3-4, pp. 443-445, ISSN 0946-2171 (Print)

Zheng L., Zhao G., Yan C., Yao G., Xu X., Su L. & Xu J. (2007). Growth and spectroscopic characteristics of Yb:LPS single crystal. *Journal of Crystal Growth*, Vol.304, No.2, pp. 441-447, ISSN 0022-0248

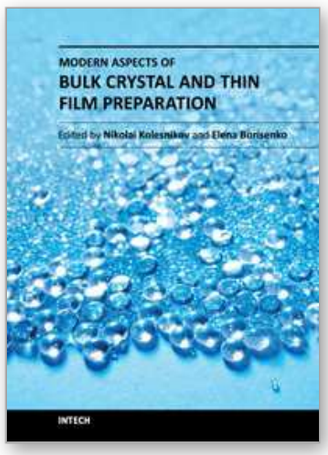

Modern Aspects of Bulk Crystal and Thin Film Preparation

Edited by Dr. Nikolai Kolesnikov

ISBN 978-953-307-610-2
Hard cover, 608 pages
Publisher InTech
Published online 13, January, 2012
Published in print edition January, 2012

In modern research and development, materials manufacturing crystal growth is known as a way to solve a wide range of technological tasks in the fabrication of materials with preset properties. This book allows a reader to gain insight into selected aspects of the field, including growth of bulk inorganic crystals, preparation of thin films, low-dimensional structures, crystallization of proteins, and other organic compounds.

How to reference

In order to correctly reference this scholarly work, feel free to copy and paste the following:

Lihe Zheng, Liangbi Su and Jun Xu (2012). Growth and Characterization of Ytterbium Doped Silicate Crystals for Ultra-Fast Laser Applications, Modern Aspects of Bulk Crystal and Thin Film Preparation, Dr. Nikolai Kolesnikov (Ed.), ISBN: 978-953-307-610-2, InTech, Available from: http://www.intechopen.com/books/modern-aspects-of-bulk-crystal-and-thin-film-preparation/growth-and-characterization-of-ytterbium-doped-silicate-crystals-for-ultra-fast-laser-applications

INTECH
open science | open minds

InTech Europe
University Campus STeP Ri
Slavka Krautzeka 83/A
51000 Rijeka, Croatia
Phone: +385 (51) 770 447
Fax: +385 (51) 686 166
www.intechopen.com

InTech China
Unit 405, Office Block, Hotel Equatorial Shanghai
No.65, Yan An Road (West), Shanghai, 200040, China
中国上海市延安西路65号上海国际贵都大饭店办公楼405单元
Phone: +86-21-62489820
Fax: +86-21-62489821

IntechOpen